Monthly Notices
of the
ROYAL ASTRONOMICAL SOCIETY

MNRAS **430,** 1832–1838 (2013) doi:10.1093/mnras/stt001

The mass of the black hole in GRS 1915+105: new constraints from infrared spectroscopy

D. J. Hurley,[1]★ P. J. Callanan,[1] P. Elebert[1] and M. T. Reynolds[2]

[1]*Department of Physics, University College Cork, Cork, Ireland*
[2]*Department of Astronomy, University of Michigan, 500 Church Street, Ann Arbor, MI 48109, USA*

Accepted 2012 December 31. Received 2012 December 25; in original form 2012 March 15

ABSTRACT

GRS 1915+105 has the largest mass function of any Galactic black hole system, although the error is relatively large. Here we present spectroscopic analysis of medium-resolution infrared Very Large Telescope archival data of GRS 1915+105 in the *K* band. We find an updated ephemeris, and report on attempts to improve the mass function by a refinement of the radial velocity estimate. We show that the spectra are significantly affected by the presence of phase-dependent CO bandhead emission, possibly originating from the accretion disc: we discuss the impact this has on efforts to better constrain the black hole mass. We report on a possible way to measure the radial velocity utilizing apparent *H*-band atomic absorption features and also discuss the general uncertainty of the system parameters of this well-studied object.

Key words: stars: individual: GRS 1915+105 – infrared: stars – X-rays: binaries.

1 INTRODUCTION

Since its discovery by Castro-Tirado et al. (1994) GRS 1915+105 remains one of the most intensively studied of all the Galactic X-ray sources, and is the prototypical Galactic 'microquasar'. This system is of particular importance, not only for our understanding of the formation of jets near black holes, but also because it is regarded as a Galactic analogue to active galactic nuclei (Mirabel & Rodríguez 1994; Castro-Tirado, Geballe & Lund 1996; Greiner et al. 2001a; Greiner, Cuby & McCaughrean 2001b). Due to its location only 0.2 arcsec from the Galactic plane, GRS 1915+105 suffers from strong interstellar absorption: the *V*-band extinction (A_V) is 19.6 ± 1.7 mag (Chapuis & Corbel 2004). For this reason observations in the *K* band have been particularly critical, leading to the identification of the secondary (Greiner et al. 2001a), a radial velocity estimate for the secondary (Greiner et al. 2001b) and the possible determination of a photometric period (Neil, Bailyn & Cobb 2007). The radial velocity study yielded a mass function of $9.5 \pm 3.0\,\mathrm{M}_\odot$ which, when combined with inclination estimates (Fender et al. 1999; Greiner et al. 2001b), indicated a primary mass of $14.0 \pm 4.0\,\mathrm{M}_\odot$. This not only confirmed the presence of a black hole in the system but also indicated it to be one the most massive black holes discovered to date in a Galactic X-ray binary. Other examples of massive primaries include Cygnus X-1 with a primary mass of $14.8 \pm 1.0\,\mathrm{M}_\odot$ (Orosz et al. 2011) and V404 Cyg, which until recently was thought to harbour a primary mass of $12 \pm 2\,\mathrm{M}_\odot$ (Shahbaz et al. 1994) but has now been reduced to $9.0^{+0.2}_{-0.6}\,\mathrm{M}_\odot$ (Khargharia, Froning & Robinson 2010).

Following the estimate by Greiner et al. (2001b), Casares (2007) noted that this mass falls outside the theoretical distribution range for our Galaxy as calculated by Fryer & Kalogera (2001). However, since the error on the black hole mass is so large ($\pm 4.0\,\mathrm{M}_\odot$), it is clear that a more accurate estimate is required before we can make a meaningful comparison to the theoretical mass distribution. In addition, McClintock et al. (2006) derive a lower limit for the dimensionless spin parameter of $a_* > 0.98$ making GRS 1915+105 a near maximally spinning Kerr black hole. This conclusion was drawn from an analysis of *RXTE* and *ASCA* data for the thermal state of GRS 1915+105, and a model of the X-ray continuum of a fully relativistic accretion disc. As discussed by McClintock et al. (2006), determining the mass of, and distance to, GRS 1915+105 is of fundamental importance for verifying this method of spin determination.

Here we present an analysis of archival Very Large Telescope (VLT) data and a re-analysis of the data presented by Greiner et al. (2001a,b). In particular, we show in what follows that, near orbital phase 0.25, the absorption lines are corrupted by emission, which will have a significant effect on the amplitude of the radial velocity variation. We discuss possible origins for this emission, and the effect it might have on the mass function and primary mass. We also discuss the feasibility of using *H*-band spectroscopy to measure the radial velocity of the secondary from narrower atomic features using new Gemini observations.

2 OBSERVATIONS

2.1 ESO VLT archival data

The European Southern Observatory (ESO) archival data used here were taken with the Infrared Spectrometer And Array

★E-mail: d.j.hurley@mars.ucc.ie

Table 1. Complete list of archival data used including total exposure times for each night in the period 1999–2002.

Date (UT)	Number of exposures	Total exposure time (s)	Phase	Date (UT)	Number of exposures	Total exposure time (s)	Phase
1999 July 23	10 × 300 s	3000	0.46271	2002 July 30	10 × 300 s	3000	0.23063
2000 April 23	8 × 240 s	1920	0.74271	2002 August 6	20 × 300 s	6000	0.43595
2000 May 11	8 × 240 s	1920	0.27410	2002 August 8	10 × 300 s	3000	0.49377
2000 May 23	8 × 240 s	1920	0.63179	2002 August 10	10 × 300 s	3000	0.55101
2000 June 10	8 × 250 s	2000	0.16171	2002 August 12	10 × 300 s	3000	0.63898
2000 June 13	8 × 250 s	2000	0.25325	2002 August 13	10 × 300 s	3000	0.64005
2000 June 18	8 × 250 s	2000	0.39898	2002 August 14	20 × 300 s	6000	0.65954
2000 July 3	8 × 250 s	2000	0.83817	2002 August 17	20 × 300 s	6000	0.75728
2000 July 9	8 × 250 s	2000	0.01589	2002 August 19	20 × 300 s	6000	0.81673
2000 July 12	8 × 250 s	2000	0.10582	2002 August 29	20 × 300 s	6000	0.11109
2000 July 14	8 × 250 s	2000	0.16342	2002 August 31	20 × 300 s	6000	0.17236
2000 July 17	8 × 250 s	2000	0.25120	2002 September 2	10 × 300 s	3000	0.22992
2000 July 23	8 × 250 s	2000	0.46333	2002 September 5	10 × 300 s	3000	0.28863
2000 July 27	8 × 250 s	2000	0.54704				
2000 August 1	8 × 250 s	2000	0.69426				
2000 August 21	8 × 250 s	2000	0.28594				

Camera (ISAAC) on the 8-m VLT Antu telescope at Cerro Paranal (Chile). The short wavelength arm of ISAAC is equipped with a 1024 × 1024 pixel Rockwell HgCdTe array with an image scale of 0.147 arcsec pixel^{-1}. Using the medium resolution grating (1.2 Å pixel^{-1} in the *K* band) yields a spectral resolution of ∼3000 with a 1 arcsec slit. Science data consisted of several 250–300 s individual exposures each night (see Table 1 for a summary of the data used). We present a re-analysis of 16 nights of observations from 2000 May to August, which were the focus of Greiner et al. (2001a,b), and 13 more from 2002 July to September which are presented here for the first time.

The bias subtraction, flat-fielding and sky subtraction were performed using the IRAF[1] CCDPROC package. The spectra were extracted using the IRAF KPNOSLIT package. Initial wavelength calibration was carried out using arc spectra obtained before or after each science run. However, cross-correlation of these spectra with the OH sky lines indicated a residual wavelength offset of ∼3–5 Å, presumably due to flexure in the telescope/spectrograph between the times when science exposures and calibration arc frames were taken. This wavelength shift was corrected for before the telluric features were removed. To correct for telluric absorption, the A0V star HD 179913 was observed either before or after the science exposures each night and the method as outlined by Vacca, Cushing & Rayner (2003) utilized.

The data were exported to MOLLY[2] where they were rebinned on to a common velocity scale. Three techniques were then used to measure the radial velocity curve: each spectrum of GRS 1915+105 was cross-correlated against (i) a template spectrum of the KIII standard star HR 8117; (ii) the average of the (remaining) spectra of GRS 1915+105; and (iii) the average of the spectra occurring around phase 0.75 (see below). All three techniques resulted in similar velocities within the errors.

As a final check, the spectra were also re-extracted using the VLT ISAAC pipeline, and the resulting radial velocities were again found to be consistent with those determined above once the shift due to instrument flexure had been removed.

[1] IRAF is distributed by the National Optical Astronomy Observatories, which are operated by the Association of Universities for Research in Astronomy, Inc., under cooperative agreement with the National Science Foundation.
[2] http://www.warwick.ac.uk/go/trmarsh/software

2.2 Gemini-North NIFS data

In Greiner et al. (2001a), the presence of atomic absorption features is identified in the *H* band. Motivated by the hope that a radial velocity measurement based on these inherently narrower features would lead to a more accurate and reliable mass function estimate, a total of three 'pathfinder' spectra were obtained using Gemini-North's Near-Infrared Integral Field Spectrometer (NIFS) on the nights of 2010 June 29, July 6 and July 13. The observations were scheduled to sample the radial velocity variation at three orbital phases. NIFS provides 3D imaging spectroscopy with a 3.0 × 3.0 arcsec^2 field of view, equipped with a 2048 × 2048 Rockwell HAWAII-2RG HgCdTe array with an image scale of 0.103 × 0.043 arcsec^2 pixel^{-1} across and along the slit. Using the H-G5604 grating and the HK-60603 filter yields a spectral resolution of ∼5000. Science data consisted of 5 × 180 s target exposures each night resulting in a signal-to-noise ratio (S/N) ∼ 24. The data were reduced using the IRAF GEMINI NIFS package and telluric absorption corrected for by observing the A0V standard star HD 182761 before and after science runs. The data were again exported to MOLLY where they were rebinned on to a common velocity scale. The spectra were then cross-correlated against the KI III template star HD 83240, taken from the catalogue of high-resolution VLT infrared spectra of Lebzelter et al. (2012). A stringent mask of the spectra was used in each case to utilize only the lines identified in Fig. 7 for the cross-correlation.

3 RESULTS

3.1 ESO VLT archival data

In Fig. 1 we plot the previously unpublished data from 2002 only, folded using the ephemeris of Greiner et al. (2001b). The maximum velocity shift is seen to occur at phase 0.5, whereas it should occur at phase 0.25 by definition, suggesting that a refinement in the ephemeris of Greiner et al. (2001b) is needed. Both the 2000 and 2002 data sets yield radial velocity amplitudes consistent with the result of 140 ± 15 km s^{-1} found by Greiner et al. (2001b), although the systemic velocity (γ) differs somewhat from the previously published value of −3 ± 10 km s^{-1}. This difference is most likely due to the skyline correction outlined in Section 2.1 as prior to this

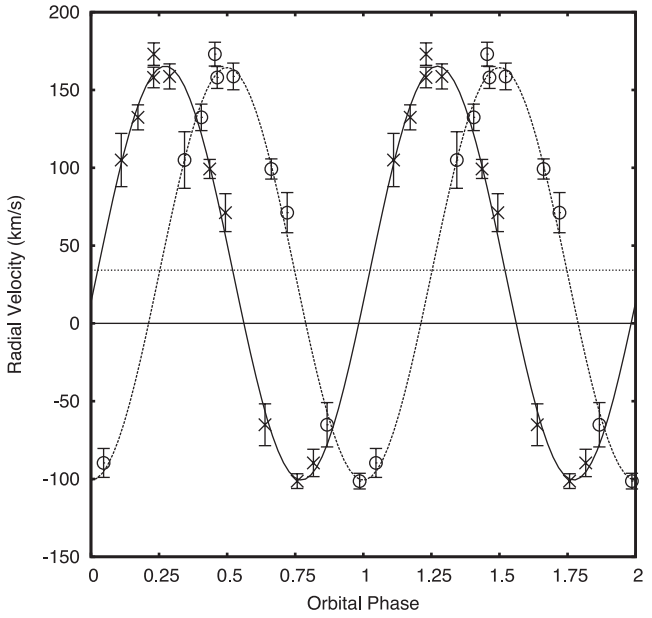

Figure 1. Radial velocity curve of the previously unpublished 2002 data set folded using the best-fitting period of Greiner et al. (2001b) $P_{\rm orb} = 33.5 \pm 1.5$ d (marked with the open circles). The fit overlaid has a reduced $\chi^2 = 1$. The peak occurs at $K_{\rm d} = 131.5 \pm 2.5$ km s^{-1} with a systemic velocity of 33.0 ± 2.1 km s^{-1}. As can be clearly seen, the phasing of the data set with the ephemeris of Greiner et al. (2001a) leads to an offset in the peak from the expected 0.25 to ∼0.5. Also plotted are the same data folded on our refined ephemeris (marked with the crosses) from the combined data set (see Fig. 3). Note that the refined ephemeris exhibits no significant offset from the expected peak of 0.25.

correction we find a systemic velocity that is consistent with that of Greiner et al. (2001b) for the same data set.

We next combined both the 2000 and 2002 data sets in order to derive an improved ephemeris by performing a period analysis via a Lomb–Scargle periodogram and then refining the results using Bretthorst's Bayesian periodogram (Bretthorst 2001) to clean out any false signals, the results of which are shown in Fig. 2 (calculated using $T_0 = 245\,1666.5$ from Greiner et al. 2001b). The peak that corresponds to a period of 33.8 ± 0.1 is the only one to successfully phase all the data consistently and so we adopt this as our revised orbital period for GRS 1915+105. This period is consistent with that of Greiner et al. (2001b) (33.5 ± 1.5 d) to within 1σ, but does not agree with the low-amplitude K-band modulation discussed by Neil et al. (2007). Folding all the data on this revised period yields the radial velocity curve shown in Fig. 3. A sine-wave fit to this plot yields a secondary radial velocity semi-amplitude ($K_{\rm d}$) of 131.9 ± 3.3 km s^{-1} and a systemic velocity (γ) of 34.2 ± 2.5 km s^{-1}. To estimate the uncertainties on derived quantities, we used a Monte Carlo analysis. This involved selecting 100 000 random samples from distributions of each input parameter i, $K_{\rm d}$, $P_{\rm orb}$ and donor mass ($M_{\rm D}$) (based on their means and standard deviations), and calculating the results based on the output distributions. Combining our initial estimates in $P_{\rm orb}$ and $K_{\rm d}$ with the suggested $M_{\rm D}$ of $0.8 \pm 0.5\,{\rm M}_{\odot}$ (Harlaftis & Greiner 2004) and the binary inclination (i) of $66^{\circ} \pm 2^{\circ}$ (Fender et al. 1999), the mass function

$$f(M) = \frac{(M_{\rm c} \sin i)^3}{(M_{\rm c} + M_{\rm D})^2} = \frac{P_{\rm orb} K_{\rm d}^3}{2\pi G}$$

is found to be $8.0 \pm 0.6\,{\rm M}_{\odot}$ (at the 68 per cent confidence interval), which is slightly lower than $9.5 \pm 3.0\,{\rm M}_{\odot}$ as determined by Greiner et al. (2001b), but consistent within their 1σ error. The mass of the primary ($M_{\rm c}$) is found to be $12 \pm 1.4\,{\rm M}_{\odot}$.

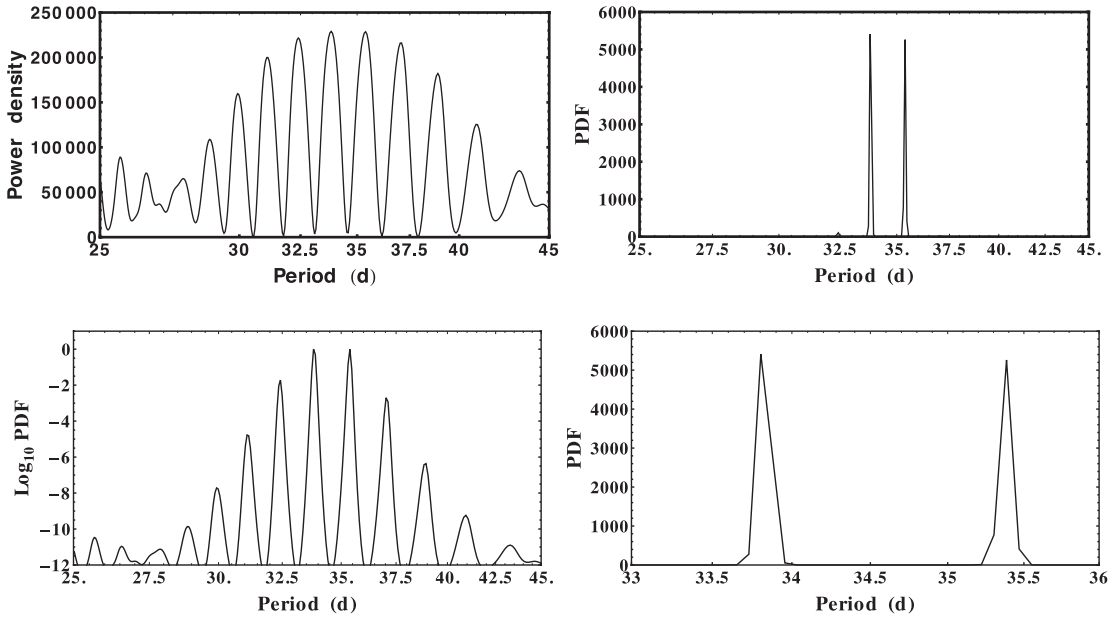

Figure 2. Top left-hand panel: Lomb–Scargle periodogram of the combined 2000 and 2002 data set with a $T_0 = 245\,1666.5$. Top right-hand panel: Bretthorst's Bayesian periodogram (Bretthorst 2001) which has been marginalized to exclude noise resulting from a non-sinusoidal source. Bottom left-hand panel: normalized log plot of the PDF to emphasize any lower peaks. Bottom right-hand panel: closer look at the two resulting major peaks which occur at 33.8 and 35.38 d, respectively, with each having a FWHM of 0.1 d which we take as the error. Of these only the 33.8 d period successfully phases both data sets correctly.

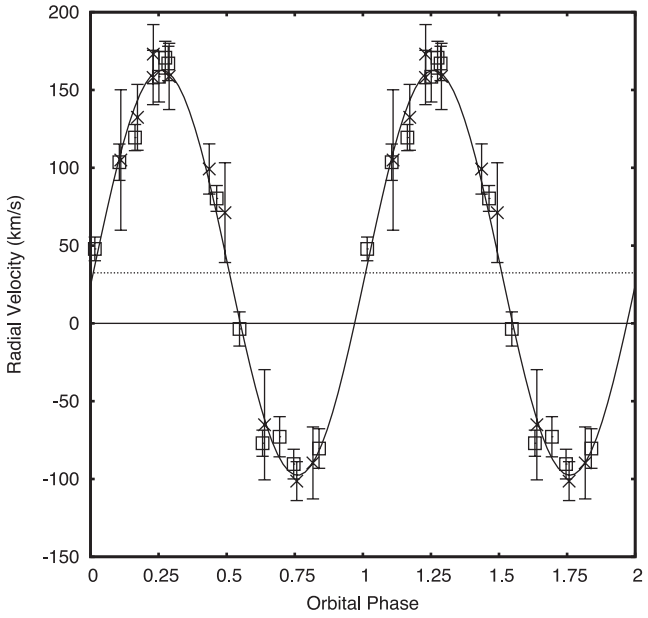

Figure 3. Radial velocity curve of the combined 2000 (marked with the open squares) and 2002 (marked with the crosses) data set folded over the best-fitting period of $P_{\rm orb} = 33.8 \pm 0.1$ d obtained from the Lomb–Scargle periodogram. The overlaid fit has a reduced $\chi^2 = 1$. The peak occurs at $K_{\rm d} = 131.9 \pm 3.3$ km s^{-1} with a systemic velocity of 34.2 ± 2.5 km s^{-1}. The scaling of error bars to produce a reduced $\chi^2 = 1$ makes the 2002 error bars larger than those in Fig. 1. This is due to the larger scatter of the points in the combined data set.

However, in Fig. 4 we plot the trailed spectra for the combined data set phased on our refined ephemeris: emission can be seen in the first half of the orbital range, indicated by the lighter regions, bluewards of all the CO bandhead absorption features (this is more apparent in the electronic colour version). The emission rises and falls over the first half of the orbit and is predominantly strongest near phase 0.25. To demonstrate this emission more clearly, in Figs 5 and 6 we plot the summed spectra, phased on the revised ephemeris, for both the 2000 and 2002 data sets. In each case, the data are further separated into two distinct orbital phase windows (0.15–0.35 and 0.65–0.85) to illustrate the presence and absence of the emission near phases 0.25 and 0.75, respectively. As can be clearly seen, there is significant CO bandhead emission present in the first half of the orbital phase range, not in the latter. This emission is present in the two epochs of observation [most noticeably near the ^{12}CO(2–0) and (3–1) transitions] indicating that it is not just a transient phenomenon. Whereas variability in the bandhead absorption had been reported by previous authors (Harlaftis & Greiner 2004), the fact that it occurs predominantly near orbital phase 0.25 has important implications for the radial velocity curve, which we discuss in Section 4.

3.2 Gemini-North NIFS data

From our NIFS spectra (see Fig. 7), we confirm the presence of many of the atomic features noted by Greiner et al. (2001a), namely: the Al triplet (λ16723.5 Å, λ16755.2 Å, λ16767.9 Å), Si I (λ15964.4 Å, λ16685.3 Å), Mg I (λ15029.1 Å, λ15044.3 Å, λ15770.1 Å, λ17113.3 Å), Fe I (λ15297.3 Å, λ15969.1 Å, λ16047.1 Å) and OH (λ16753.8 Å). Equivalent widths (EWs) of some of the major lines can be found in Table 2. We do not detect Br series (λ or η), CO or He I. We first used these spectra to independently estimate the effective temperature ($T_{\rm eff}$) of the secondary, from equation (3) of Le et al. (2011), using the EW of the Mg I (λ17113.3 Å) line. From this we estimate an $T_{\rm eff}$ of 4540^{+505}_{-505} K which is reassuringly consistent with the K2 III classification already ascribed by Greiner et al. (2001a).

The resulting velocities from our cross-correlation analysis (see Section 2.2 for details) are shown in Table 2.These were then searched for the expected variation due to the motion of the secondary, based on the results of the *K*-band observations outlined in Section 3.1. However, even with the improvement in the error of the ephemeris (Section 3.1), over the intervening 110 cycles between the *K*- and *H*-band observations the uncertainty in phase information accumulates to $\sim\pm0.33$. Hence, in constraining $K_{\rm d}$, the absolute phase was left as a free parameter. We used the γ velocity found in Section 3.1. To our surprise, we do not find the radial velocity variation expected, based on the CO bandhead measurements discussed in Section 3.1 and Greiner et al. (2001b). Our measurements are consistent only with an upper limit of $\sim$50 km s^{-1} on $K_{\rm d}$, although this depends strongly on the assumed value of γ.

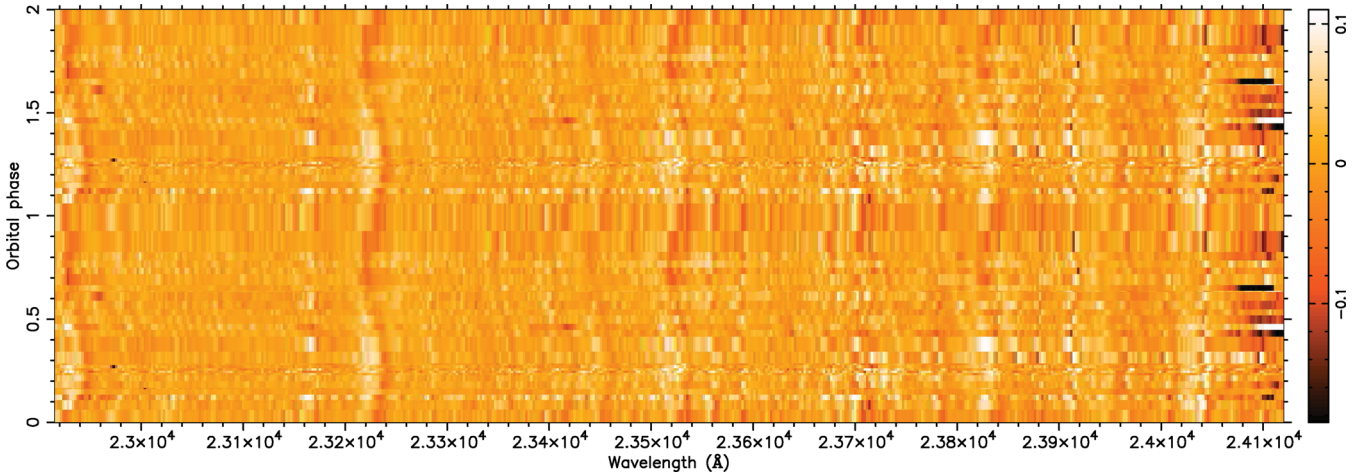

Figure 4. Trailed spectrum of all data, repeated twice for clarity. The lighter colours indicate emission and darker absorption. Notice the emission is visible only in the first half of the orbital cycle, bluewards of each bandhead, and is strongest near phase ∼0.25 (see the electronic version also). Intermittent emission at λ23160 Å is a residual telluric feature.

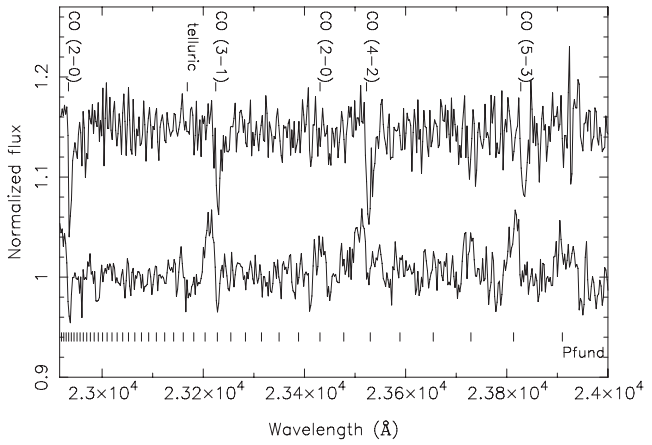

Figure 5. Bottom panel: average of 2000 spectra between 0.15 and 0.35 in phase. Top panel: average of 2000 spectra taken between 0.65 and 0.85. Notice the emission present in the former compared to the latter. The positions of the Pfund lines are indicated to demonstrate that they cannot account for the structure of the observed emission.

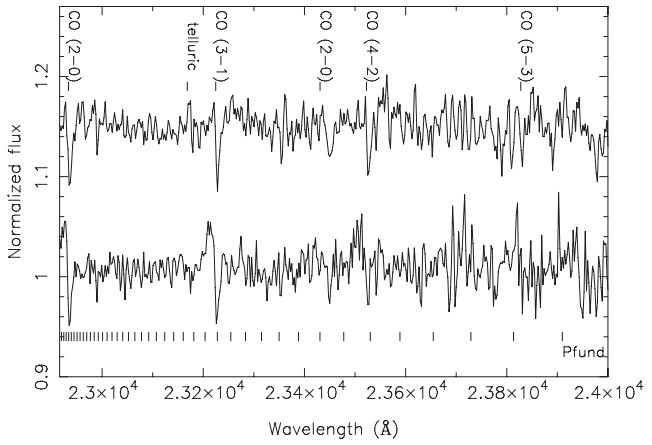

Figure 6. Bottom panel: average of 2002 spectra between 0.15 and 0.35 in phase. Top panel: average of 2002 spectra taken between 0.65 and 0.85. Again, as with the 2000 spectra, the emission is present in the same orbital ranges. Again, the positions of the Pfund lines are indicated for reference.

4 DISCUSSION

4.1 *H*-band atomic absorption

It is clear that some caution should be used when interpreting the radial velocity variation (or lack thereof) in the *H* band, as we have only three measurements at our disposal. If the lack of variation (compared to what is expected from the *K*-band) is real, then we must look for alternative sources of the *H*-band emission. For example, the work of Muno, Morgan & Remillard (1999) and Lee et al. (2002) suggests that GRS 1915+105 may possess a circumbinary disc of material: if we assume such a disc is the source of the *H*-band absorption features, then we can use the full width at half-maximum (FWHM) of the latter to constrain the location of the emission. The observed FWHM of the absorption features is $\sim$60 km s^{-1}, and assuming a Keplerian disc orbiting a binary of total mass 12.8 $M_{\odot}$, we estimate a radius of 530 $R_{\odot}$, well outside the binary radius of 100 $R_{\odot}$. However, it remains suspicious that the *H*-band spectrum, despite the lack of radial velocity variation, so closely matches the expected spectral type of the secondary. It is clear that more systematic observations of these spectral features are warranted.

4.2 CO bandhead emission

The CO emission is a rare phenomenon in accreting binary systems: to our knowledge, it has only previously been observed in the well-known cataclysmic variable WZ Sagittae (Howell, Harrison & Szkody 2004). As with Howell et al. (2004), we also believe that H Pfund emission is unlikely to be a major contributor to the observed emission. Higher order lines ($>P33$) blend to form a continuum at shorter wavelengths (see Fig. 5) and do not exhibit the discrete band structure bluewards of each CO bandhead that is observed. Also, the intensity of Pfund emission lines should increase from shorter to longer wavelengths, whereas the emission that we observe is approximately uniform at each site. Hence, we believe that CO bandhead emission is the best explanation for the observed emission features.

With a dissociation energy of 11.1 eV, the site of this emission must reside in a relatively cool, outer part of the disc. Such a region cannot be directly illuminated by X-rays from the inner disc, and must instead be shielded from it. This could be provided, for example, by a warped accretion disc, which in turn has been invoked to explain the long-term periodicities in the X-ray light curve of GRS 1915+105 (Rau, Greiner & McCollough 2003).

However, it is the fact that the emission occurs preferentially near orbital phase 0.25 which most interests us here. Such emission may become more visible near this phase because the absorption lines of the secondary are at their maximum redshift at this phase, making emission from the accretion disc easier to observe. However, the same should be true at maximum blueshift (phase 0.75), which is not the case for our data.

Alternatively, it may simply be that the shielded region of the disc is best visible near binary phase 0.25 – although, in the context of a warped and precessing disc (Lee et al. 2002), it is not clear why this should be the case for both epochs of observations. Another possible cause for the appearance of the blueshifted emission phenomenon is P Cygni type emission originating from a wind-driven outflow of material, such as proposed by Lee et al. (2002) for GRS 1915+105. This would imply a shell of material somewhere between 200 and 400 $R_{\odot}$ from the primary (Clark et al. 1999, equation 1). The dominant source of uncertainty for this estimate, however, is due to the uncertainty in the distance to the binary.

The uncertainty in the distance to GRS 1915+105 also plays a significant role in any attempt to tightly constrain the black hole mass. This is because the estimate for the primary mass stated in Section 3.1 relies heavily on the inclination of the system. While cited by many authors as $66^{\circ} \pm 2^{\circ}$ (McClintock et al. 2006; van Oers et al. 2010; Rahoui et al. 2010), this estimate is based in turn on an accurately known distance. However, the distance to GRS 1915+105 is still a matter of some debate; the conservative estimate of 9.0 ± 3.0 kpc as proposed by Chapuis & Corbel (2004) would suggest a binary inclination of $58^{\circ} \pm 11^{\circ}$ (using equation 4 from Fender et al. 1999). Combining this with a donor mass of $0.8 \pm 0.5\,M_{\odot}$ (Harlaftis & Greiner 2004) yields a considerably more uncertain primary mass of $16.7 \pm 7.4\,M_{\odot}$.

To estimate the distance to GRS 1915+105, Greiner et al. (2001b) combined their estimate of γ with the Galactic rotation curve of Fich, Blitz & Stark (1989) to yield $D = 12.1 \pm 0.8$ kpc. Using

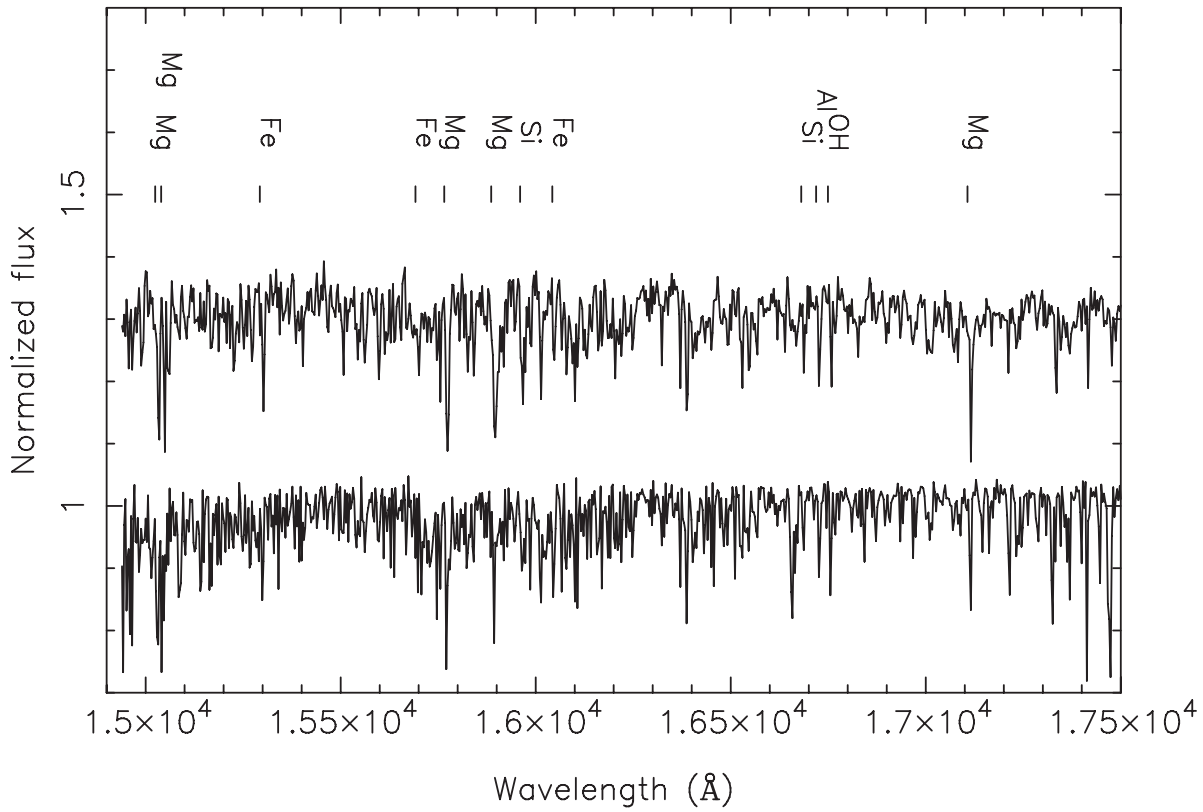

Figure 7. *H*-band spectrum confirming the presence of atomic features. Top panel: spectrum from a single night's observation with Gemini. All features indicated are found in each of the three spectra. EWs of selected lines can be found in Table 2. Bottom panel: template star HD 83240 from the catalogue of Lebzelter et al. (2012).

Table 2. EWs of *H*-band spectra. Only the deepest lines are listed. Also listed are the corresponding radial velocity measurements, and their associated errors, from the cross-correlation analysis in MOLLY.

Spectrum	Mg (15770.9) (Å)	Si (1668.53) (Å)	Mg (17113.08) (Å)	Al (16723.5) (Å)	Velocity (km s^{-1})
2010 June 29	2.02 ± 0.16	0.59 ± 0.10	1.07 ± 0.10	1.25 ± 0.22	9.1 ± 20.5
2010 July 06	2.47 ± 0.15	0.44 ± 0.10	0.92 ± 0.10	1.31 ± 0.15	54.4 ± 21.3
2010 July 13	2.55 ± 0.15	0.49 ± 0.10	1.05 ± 0.11	1.07 ± 0.13	62.5 ± 21.9
HD 83240	2.23 ± 0.20	0.47 ± 0.10	0.99 ± 0.09	0.567 ± 0.07	

the same technique, our estimate of γ (see Section 3.1) yields $D = 9.4 \pm 0.2$ kpc, where the low error is due to the fact that we assume a flat rotation curve and thereby only the uncertainty on γ contributes. This in turn would suggest an inclination of $62^\circ \pm 2^\circ$ (again from Fender et al. 1999), and a primary mass of $12.9 \pm 2.4\,M_\odot$.

Finally, it is also clear that the black hole mass estimate will also be affected by the presence of the bandhead emission. Specifically, near phase 0.25, the absorption line measurements will be skewed to higher velocities, artificially increasing the amplitude of the radial velocity curve. In addition, the presence of the bandhead emission will also affect the measurement of γ in the same manner. Hence, in this sense, the mass function we have derived must be considered an upper limit only. Further attempts to refine the mass function and γ of GRS 1915+105 utilizing *K*-band spectroscopy will depend on the feasibility of decontaminating the absorption features from this emission contribution, especially near phase 0.25. This will require higher resolution and S/N spectra than have been obtained thus far.

5 CONCLUSIONS

We have confirmed the presence of narrow atomic features in the *H* band as noted by Greiner et al. (2001a), but our analysis does not provide evidence for the expected radial velocity variation. This may suggest that the origin of the absorption is distinct from the secondary and outside the binary but more observations are clearly required to confirm this. Alternatively, the CO bandhead emission observed specifically at phase 0.25 brings into question the reliability of the radial velocity amplitude of the secondary based on the *K*-band observations. Higher resolution *K*-band observations are required to disentangle the emission from the bandhead absorption so that a reliable radial velocity estimate can be made.

ACKNOWLEDGEMENTS

We gratefully acknowledge the use of the MOLLY software package developed by T. Marsh. We would also like to thank the

anonymous referee for useful suggestions leading to an improved paper.

REFERENCES

Bretthorst G. L., 2001, in Mohammad-Djafari A., ed., AIP Conf. Ser. Vol. 568, Bayesian Inference and Maximum Entropy Methods in Science and Engineering: 20th International Workshop. Am. Inst. Phys., New York, p. 241
Casares J., 2007, in Karas V., Matt G., eds, Proc. IAU Symp. 238, Black Holes from Stars to Galaxies – Across the Range of Masses. Cambridge Univ. Press, Cambridge, p. 3
Castro-Tirado A. J., Brandt S., Lund N., Lapshov I., Sunyaev R. A., Shlyapnikov A. A., Guziy S., Pavlenko E. P., 1994, ApJS, 92, 469
Castro-Tirado A. J., Geballe T. R., Lund N., 1996, ApJ, 461, L99
Chapuis C., Corbel S., 2004, A&A, 414, 659
Clark J. S., Steele I. A., Fender R. P., Coe M. J., 1999, A&A, 348, 888
Fender R. P., Garrington S. T., McKay D. J., Muxlow T. W. B., Pooley G. G., Spencer R. E., Stirling A. M., Waltman E. B., 1999, MNRAS, 304, 865
Fich M., Blitz L., Stark A. A., 1989, ApJ, 342, 272
Fryer C. L., Kalogera V., 2001, ApJ, 554, 548
Greiner J., Cuby J., McCaughrean M., Castro-Tirado A., Mennickent R., 2001a, A&A, 373, L37
Greiner J., Cuby J., McCaughrean M., 2001b, Nat, 414, 522
Harlaftis E. T., Greiner J., 2004, A&A, 414, L13
Howell S. B., Harrison T. E., Szkody, 2004, ApJ, 602, L49
Khargharia J., Froning C. S., Robinson E. L., 2010, ApJ, 716, 1105
Lebzelter T. et al., 2012, A&A, 539, A109
Le H. A. N., Kang W., Pak S., Im M., Lee J. E., Ho L. C., Pyo T. S., Jaffe D. T., 2011, J. Korean Astron. Soc., 44, 125
Lee J. C., Reynolds C. S., Remillard R., Schulz N. S., Blackman E. G., Fabian A. C., 2002, ApJ, 567, 1102
McClintock J. E., Shafee R., Narayan R., Remillard R. A., Davis S. W., Li L. X., 2006, ApJ, 652, 518
Mirabel I. F., Rodríguez L. F., 1994, Nat, 371, 46
Muno M. P., Morgan E. H., Remillard R. A., 1999, ApJ, 527, 321
Neil E. T., Bailyn D., Cobb B. E., 2007, ApJ, 647, 409
Orosz J. A., McClintock J. E., Aufdenberg J. P., Remillard R. A., Reid M. J., Narayan R., Gou L., 2011, ApJ, 742, 84
Rahoui F., Chaty S., Rodriguez J., Fuchs Y., Mirabel I. F., Pooley G. G., 2010, ApJ, 715, 1191
Rau A., Greiner J., McCollough M. L., 2003, ApJ, 590, L37
Shahbaz T., Ringwald F. A., Bunn J. C., Naylor T., Charles P. A., Casares J., 1994, MNRAS, 271, L10
Vacca W. D., Cushing M. C., Rayner J. T., 2003, PASP, 115, 389
van Oers P. et al., 2010, MNRAS, 409, 763

This paper has been typeset from a TEX/LATEX file prepared by the author.